

Influence of spin fluctuations on the superconducting transition temperature and resistivity in the $t - J$ model at large N

A. Greco^{a,b} and R. Zeyher^a

^a *Max-Planck-Institut für Festkörperforschung,
Heisenbergstr.1, 70569 Stuttgart, Germany*

^b *Permanent address: Departamento de Física, Facultad de Ciencias Exactas e Ingeniería and
IFIR(UNR-CONICET), Av. Pellegrini 250, 2000-Rosario, Argentina*
(October 25, 2018)

Abstract

Spin fluctuations enter the calculation of the superconducting transition temperature T_c only in the next-to-leading order (i.e., in $O(1/N^2)$) of the $1/N$ expansion of the $t - J$ model. We have calculated these terms and show that they have only little influence on the value for T_c obtained in the leading order $O(1/N)$ in the optimal and overdoped region, i.e., for dopings larger than the instability towards a flux phase. This result disagrees with recent spin-fluctuation mediated pairing theories. The discrepancies can be traced back to the fact that in our case the coupling between electrons and spins is determined by the t - J model and not adjusted and that the spin susceptibility is rather broad and structureless and not strongly peaked at low energies as in spin-fluctuation models.

Relating T_c and transport we show that the effective interactions in the particle -particle and particle-hole channels are not simply related within the $1/N$ expansion by different Fermi surface averages of the same interaction as in the case of phonons or spin fluctuations. As a result, we find that large values for T_c and rather small scattering rates in the normal state as found in the experiments can easily be reconciled with each other. We also show that correlation effects heavily suppress transport relaxation rates relative to quasiparticle relaxation rates in the case of phonons but not in the case of spin fluctuations.

PACS numbers: 74.20-z, 74.20.Mn, 74.25.Ha

I. INTRODUCTION

Calculations of the superconducting transition temperature T_c and other specific properties of the cuprates are usually based on the Hubbard model. One approach assumes that the effective Hubbard repulsion U is smaller or comparable to the electronic hopping amplitude t so that approximations which become exact at weak coupling are taken as a basis for calculations of properties of the cuprates. The FLEX approximation¹, which sums bubble and ladder diagrams in a self-consistent way, is such an approximation which has been rather successful in reproducing properties of the cuprates². A rather different and certainly more realistic view of the cuprates assumes that U is substantially larger than t at all relevant dopings. As a result the strong-coupling limit of the Hubbard model applies which is equivalent, except for three-center potentials, to the $t - J$ model. Cuprates are then no longer treated as moderately correlated metals as in the FLEX approximation but as doped Mott insulators. Formally this means that self-energies, effective interactions, etc., are not expanded in powers of U but in $1/U$ and that, as a new point, the constraint of having no double occupancies of sites has to be taken into account. Throughout our paper we adopt this second point of view and thus assume that the strong-coupling limit applies to the cuprates over the whole doping region including also the overdoped case.

The $t - J$ model has no small parameter which would allow a systematic perturbation expansion. One way out is to extend this model in such a way that a small parameter arises and that the properties of the original model are obtained as power expansion in this small parameter. One convenient generalization consists of replacing the two spin components of the $t - J$ model by N components and, correspondingly, its original $SU(2)$ symmetry by the symplectic symmetry group $Sp(N/2)$. In this way properties of the physical $N = 2$ model can be expanded around the $N = \infty$ limit of the extended model which describes renormalized, but non-interacting, particles. The interaction between the particles can then be taken into account by means of a systematic $1/N$ expansion. We have formulated this expansion directly in terms of X -operators which respect the constraint via their commutator and anticommutator rules. Applying this method to superconducting instabilities we found³⁻⁵ for a square lattice relevant instabilities only in the d-wave channel (Γ_3 representation of the point group C_{4v} of the square lattice) due to the Heisenberg term. Putting $N = 2$, the corresponding transition temperature T_c was about 0.03 in units of the nearest-neighbor hopping element t for a doping value away from half-filling of $\delta = 0.17$.

The above calculation took into account only the leading order of the $1/N$ expansion. Thus the anomalous self-energy was calculated in $O(1/N)$, or equivalently, the kernel Θ of the linearized gap equation in $O(1)$, since an overall factor $1/N$ has been taken out in the gap equation (see Eq.(40) of Ref.⁵, or Eq.(1) below). Although this order contains also spin-flip contributions it does not contain the well-known RPA terms for the spin susceptibility. These terms are, of course, present in the $1/N$ expansion but their leading contribution (one bubble) yields only $1/N$ terms to Θ and thus has been dropped in Ref.⁵.

Presently many experimental data are interpreted as giving evidence for a spin-fluctuation mediated pairing mechanism for high- T_c superconductivity⁶⁻⁹. It is thus interesting to include the above terms, at least, if they are of $O(1/N)$ in Θ , in the calculation of T_c . It is the aim of the present communication to do this and to consider their effects on T_c and the resistivity. Using the $1/N$ expansion of the $t - J$ model these terms can

easily be identified. The corresponding coupling strength between electrons and spins is determined uniquely by the model parameters and has not to be chosen in an ad hoc way. At the same time such a calculation yields a check for the validity of the $1/N$ expansion for T_c : If, for instance, the next-to-leading terms are of the same magnitude as the leading ones, after putting $N = 2$, a rapid convergence of the series cannot be expected. Of course, the comparison of the two orders would be most convincing if all the $O(1/N)$ terms of Θ could be taken into account. The resulting expressions are, however, rather involved and their evaluation has to be postponed. In the following we will restrict ourselves to that part of Θ , called Θ_s , which is of $O(1/N)$ and describes RPA-like spin fluctuations. These terms are derived in section 2. Section 3 discusses properties of the resulting spin susceptibility and compares them with a different theoretical approach and also with experimental data. In section 4 properties of Θ_s , which are relevant for superconductivity, are discussed and their influence on T_c is calculated. In section 5 the consequences of Θ for transport properties are investigated. Section 6 contains our conclusions. Throughout the paper we will restrict ourselves to dopings $\delta > \delta_c$ where δ_c denotes the critical value for the instability towards a flux or bond-order phase^{4,5,10,11}. δ_c is about 0.15 for $J/t = 0.3$. It has been argued¹¹ that δ_c corresponds to optimal doping so that we deal in the following with optimal doping and the overdoped regime.

II. BASIC EQUATIONS

Using a $1/N$ expansion for the $t-J$ model the linearized equation for the superconducting gap Σ_{an} can be written as⁵

$$\Sigma_{an}(k) = -\frac{T}{NN_c} \sum_{k'} \Theta(k, k') \frac{1}{\omega_{n'}^2 + \epsilon^2(\mathbf{k}')} \Sigma_{an}(k'). \quad (1)$$

N denotes the number of electronic degrees of freedom per site. We assume that they consist of $N/2$ replica of one orbital with two spin components and N can be assumed to be an even integer for convenience. N_c is the number of primitive cells and k the supervector $k = (\omega_n, \mathbf{k})$, where ω_n denotes the fermionic Matsubara frequency $\omega_n = (2n + 1)\pi T$, \mathbf{k} the wave vector, and T the temperature. $\epsilon(\mathbf{k})$ is the one-particle energy

$$\epsilon(\mathbf{k}) = \frac{\delta}{2}t(\mathbf{k}) - J(\mathbf{k}) \cdot \frac{1}{N_c} \sum_{\mathbf{p}} \cos(p_x) f(\epsilon(\mathbf{p} - \mu)), \quad (2)$$

with

$$t(\mathbf{k}) = -2|t|(\cos(k_x) + \cos(k_y)), \quad (3)$$

$$J(\mathbf{k}) = 2J(\cos(k_x) + \cos(k_y)). \quad (4)$$

μ is the chemical potential, f the Fermi function, δ the doping away from half filling and the lattice constant of the square lattice has been put to one. Note also that the usual definition of the hopping matrix element in $N = 2$ theories corresponds to $|t|/2$ in our notation. Generally accepted values for $|t|/2$ and J are about 0.4eV and 0.15eV , respectively. In the

following we will use $|t|/2$ as energy unit. The kernel Θ represents the effective interaction in the particle-particle channel. Its leading $O(1)$ contributions consist of four different terms $\Theta^{(1)}$, $\Theta^{(2)}$, $\Theta^{(3)}$, and $\Theta^{(4)}$, given explicitly in Eqs.(42)-(52) of Ref.⁵. The first one describes the instantaneous part, the second one fluctuations in the charge density, and the third and fourth ones mixed spin and charge fluctuations due to the anomalous part of the vertex.

$\Theta^{(2)}$ originates from single particle and collective electron-hole excitations in the charge channel. A similar contribution Θ_s is also obtained in the spin channel

$$\Theta_s(k, k') = -(t(\mathbf{k}') + J(\mathbf{k} - \mathbf{k}'))\gamma_s(k, k' - k), \quad (5)$$

where the sign for singlet pairing has been chosen. Expanding γ_s in powers of $1/N$ the leading $O(1)$ contribution is just a product of delta-functions. This contribution has already been taken into account in $\Theta^{(1)}$. The $O(1/N)$ contribution of γ_s contains the term

$$\gamma'_s(k_1, k_2) = \frac{1}{N}(t(\mathbf{k}_1) + J(\mathbf{k}_2))\chi^{(0)}(k_2), \quad (6)$$

with

$$\chi^{(0)}(k) = \frac{1}{N_c} \sum_{\mathbf{q}} \frac{f(\epsilon(\mathbf{k} + \mathbf{q})) - f(\epsilon(\mathbf{q}))}{\epsilon(\mathbf{k} + \mathbf{q}) - \epsilon(\mathbf{k}) - i\omega_n}. \quad (7)$$

Inserting Eq.(6) into Eq.(5) we have the following additional $O(1/N)$ contribution to the kernel Θ_s due to spin fluctuations

$$\Theta_s(k_1, k_2) = -\frac{1}{N}(t(\mathbf{k}_2) + J(\mathbf{k}_1 - \mathbf{k}_2))(t(\mathbf{k}_1) + J(\mathbf{k}_1 - \mathbf{k}_2))\chi^{(0)}(k_1 - k_2). \quad (8)$$

Both the susceptibility $\chi^{(0)}$ and the coupling functions on the right-hand side of Eq.(8) are different from what one may expect from a simple spin-fluctuation mediated theory for superconductivity. The coupling functions (first and second factors in the above expression) contain not only the potential J but also the kinetic parameter t . The origin of the latter lies in the fact that fermionic Hubbard operators are not usual creation and annihilation operators and generate many-body interactions in the perturbation expansion. Secondly, one would expect the RPA expression for the spin susceptibility on the right-hand side of Eq.(8) and not the equivalent of just one bubble, as described by Eq.(7). The reason for this is that in RPA-type diagrams each bubble is multiplied by J/N , i.e., entering as an $O(1/N)$ contribution. Thus the infinite summation over bubbles in the RPA is not in the spirit of the $1/N$ expansion: Before the product of even two bubbles can be included one has to sum up infinite series of diagrams of different types. This can be seen from the $O(1/N)$ expression for the spin vertex γ_s in Refs.^{12,13}. Since $\chi^{(0)}$ already exhausts more than half of the exact sum rule for the spin susceptibility (see below) we retain from the $O(1/N)$ terms to Θ only the term Θ_s , as given by Eq.(8).

III. SUM RULE AND PROPERTIES OF THE SPIN SUSCEPTIBILITY

For a general N the spin operator at site i is replaced by

$$S_i^\alpha \rightarrow S_i^\alpha(\nu), \quad (9)$$

where ν is a flavor index counting the $N/2$ copies of the original orbital and α a Cartesian index counting the three vector components of the spin. Expressed by Hubbard operators the z-component of the spin operator acting on the copy ν reads

$$S_i^z(\nu) = \frac{1}{2}(X_i^{2\nu,2\nu} - X_i^{1\nu,1\nu}). \quad (10)$$

The spin susceptibility $\chi^{\alpha\beta}$ is defined in Fourier space for a general N by

$$\chi^{\alpha\beta}(\mathbf{k}, \omega) = \frac{2}{N} (-i) \sum_{\nu=1 \dots N/2} \int_0^\infty dt e^{i\omega t} \langle [S_{\mathbf{k}}^\alpha(t, \nu), S_{-\mathbf{k}}^\beta(0, \nu)] \rangle, \quad (11)$$

where $\langle \dots \rangle$ denotes a thermodynamic average and $[\dots]$ the commutator. Inserting Eq.(10) into Eq.(11), using the fluctuation-dissipation theorem, summing over \mathbf{k} and integrating over ω we obtain for the z-component of the imaginary part of χ in the normal state

$$-\frac{1}{N_c} \sum_{\mathbf{k}} \int_{-\infty}^\infty Im \chi^{zz}(\mathbf{k}, \omega) (1 + n(\omega)) = \frac{\pi}{2N} \sum_{\nu=1 \dots N/2} \langle (X_i^{2\nu,2\nu} - X_i^{1\nu,1\nu})^2 \rangle. \quad (12)$$

$n(\omega)$ is the Bose function. The right-hand side of Eq.(12) can be evaluated exactly for the two cases $N = 2$ and $N = \infty$. For $N = 2$, which corresponds to the physical case of one orbital with two spin components, the X -operators are projection operators, so that Eq.(12) becomes, using also the constraint $X_i^{00} + X_i^{11} + X_i^{22} = 1$,

$$-\frac{1}{N_c} \sum_{\mathbf{k}} \int_{-\infty}^\infty d\omega Im \chi^{zz}(\mathbf{k}, \omega) (1 + n(\omega)) = \frac{\pi}{4}(1 - \delta), \quad (13)$$

where δ is the doping away from half-filling. Eq.(13) is exact and generalizes the spin sum rule to a general doping δ . Experimental data are usually given in terms of the magnetic susceptibility which is the product of the spin susceptibility and $g^2\mu_B^2$, where g and μ_B are the gyromagnetic ratio and the Bohr magneton, respectively. Following a widely used notation we denote the negative imaginary part of the magnetic susceptibility, analytically continued to the real axis $i\omega_n \rightarrow \omega + i\eta$, by $\chi''(\mathbf{k}, \omega)$. Inserting $g = 2$ the sum rule Eq.(13) assumes then the form

$$\frac{1}{N_c} \sum_{\mathbf{k}} \int_{-\infty}^\infty d\omega \chi''(\mathbf{k}, \omega) (1 + n(\omega)) = \mu_B^2 \pi (1 - \delta). \quad (14)$$

For $N > 2$ the projection properties of the X operators are lost and non-diagonal averages on the right-hand side of Eq.(12) are nonzero. However, at large N 's the non-diagonal averages are by a factor $1/N$ smaller than the diagonal ones and thus can be omitted. The diagonal ones can be calculated using Eq.(7) and one obtains instead of Eq.(14)

$$\frac{1}{N_c} \sum_{\mathbf{k}} \int_{-\infty}^\infty d\omega \chi''(\mathbf{k}, \omega) (1 + n(\omega)) = \mu_B^2 \pi (1 - \delta^2)/2. \quad (15)$$

At large dopings Eqs.(14) and (15) agree approximately but at zero doping the right-hand side of Eq.(15) is only $1/2$ of that of Eq.(14). The right-hand side of the above sum rules,

considered as a function of N , interpolates between the above two extreme cases $N = 2$ and $N = \infty$. This means that terms $\sim 1/N$ and of higher orders contribute to the sum rule and, if evaluated at $N = 2$, cancel the factor $(1 + \delta)/2$ on the right-hand side of Eq.(15). This implies, in particular, that the sum rule for the spin susceptibility depends on the strength of the interaction between the particles.

Fig. 1 shows theoretical and experimental data for the momentum averaged magnetic susceptibility $\chi''(\omega)$, defined by

$$\chi''(\omega) = \frac{1}{N_c} \sum_{\mathbf{k}} \chi''(\mathbf{k}, \omega). \quad (16)$$

The dot-dashed line represents the susceptibility at large N 's, $\chi''_{\infty}(\omega)$. The dashed curve in Fig. 1 is a plot of the function $\chi''_P(\omega)$ which is associated with the following phenomenological expression for the spin susceptibility in high- T_c compounds^{6–8},

$$\chi_P(\mathbf{k}, \omega) = \frac{\chi_Q}{-i\omega/\omega_{sf} + (1 + \xi^2(\mathbf{k} - \mathbf{Q})^2)}. \quad (17)$$

Here we have used the values listed in Table II of Ref.⁸ for the various parameters for $\delta = 0.2$ (second-last column in Table II). The open circles in Fig. 1 are experimental points for the momentum averaged susceptibility divided by 2 in underdoped $YBaCu_3O_{6.6}$ ¹⁴ at $T = 80K$. Analogous experimental data have been presented in Refs.^{15–17} for various dopings in $YBa_2Cu_3O_{7-x}$. The data for $YBa_2Cu_3O_{6.7}$ (Fig. 6 of Ref.¹⁷), covering the energy window between 0 and 70 meV, are smaller by roughly a factor 2, but otherwise rather similar: They also show a first maximum at around 30 meV and a second maximum, which lies at a somewhat lower energy of about 60 meV and is broader and less pronounced compared to the experimental data shown in Fig. 1. Increasing the doping in $YBa_2Cu_3O_{7-x}$ spin scattering in the normal state becomes weaker and finally undetectable in the optimally doped case¹⁷. χ''_{∞} exhausts a little more than half of the sum rule Eq.(12). It spreads in frequency over the bandwidth of about 0.7 eV and exhibits a broad maximum near 0.3 eV. Integrating $\chi''_{\infty}(1 + n(\omega))$ up to the largest measured frequency the dot-dashed and the experimental curve exhaust about 1/6 of the sum rule¹⁸. However, the experimental points for the oxygen contents 6.6 and 6.7 show a dramatic shift of spectral weight from high to low frequencies which is absent in χ''_{∞} . The dashed curve in Fig. 1 is of similar magnitude as the experimental curve between 0 and about 70 meV. However, it misses the strong decrease of the experimental curve above 70 meV and is therefore much too large at high frequencies.

Fig. 2 shows data for $\chi''(\mathbf{Q}, \omega)$ at $\mathbf{Q} = (\pi, \pi)$ where the susceptibilities assume either their maximal values in \mathbf{k} -space or are near their maximal values in case where a splitting into incommensurate peaks positioned near \mathbf{Q} occurs. The filled circles are experimental values from Ref.¹⁷ for $YBa_2Cu_3O_{6.7}$ at $T = 200K$. The dot-dashed and dashed curves in Fig. 2 represent $\chi''_{\infty}(\mathbf{Q}, \omega)$, multiplied by 10, and $\chi''_P(\mathbf{Q}, \omega)$, respectively. Note that there is a scale change of about a factor 50 along the y-axis between Figs. 1 and 2. This means that the experimental spectral weight of the spin susceptibility is strongly concentrated near \mathbf{Q} and at low energies around 20 or 30 meV. This strong localization in momentum and energy is absent to a large extent in χ''_{∞} and to a minor degree also in χ''_P . Plotted as a function of momentum for a fixed frequency χ''_{∞} shows well-pronounced incommensurate peaks near \mathbf{Q} in spite of the fact that $\chi''_{\infty}(\mathbf{Q}, \omega)$ as a function of ω is according to Fig. 2 rather small and structureless.

The showing of experimental points for the underdoped regime in Figs. 1 and 2 does not mean that χ''_∞ should reproduce these experimental spectra. As mentionned in the introduction our $1/N$ expansion holds in this form only for dopings δ larger than δ_c where the instability towards a flux phase occurs, i.e., as discussed in Ref.¹¹, in the optimally doped and overdoped region. Presently spin scattering in optimally doped $YBa_2Cu_3O_7$ is too weak to be detectable by inelastic neutron scattering with the instrumentation currently available¹⁷. Recently, an upper limit for $\chi''(\mathbf{Q}, \omega)$ of $45\mu_B^2/eV$ has been given for the instrumentally accessible energy range $20meV < \omega < 50meV$ ¹⁹ which is substantially lower than the dashed line in Fig. 2. This suggests that a low-frequency peak in χ'' is present only at low dopings and that χ'' in optimally doped and overdoped samples extends over a large energy region because of the exact sum rule Eq.(13). One thus may argue that χ''_∞ may represent well the spin susceptibility in the optimal and overdoped regimes and that the experimental points as well as χ''_P in Figs.1 and 2 only apply to the underdoped case.

Another quantity characterizing χ is the coherence length ξ . In an isotropic two-dimensional description the decay of the the real part of $\chi(\mathbf{r}, \omega = 0)$ in real space is given by $K_0(|\mathbf{r}|/\xi)$, where K_0 is a modified Bessel function of zeroth order. The dashed and dot-dashed lines in Fig. 3 represent this Bessel function for $\xi = 2.3$ and $\xi = 1.0$, respectively. The diamonds are the absolute values for the real part using χ_P at various neighbor sites of the square lattice. The diamonds lie perfectly on the Bessel function with $\xi = 2.3$ as expected. The circles in Fig. 3 have been calculated with the large-N susceptibility χ_∞ . Because of the anisotropy of the lattice not all of the calculated points lie on the curve for the Bessel function. Fig. 3 nevertheless shows that the corresponding ξ is near the value 1. Repeating the same calculation at finite temperatures we find that ξ varies with temperature on the scale of t and thus is independent of temperature in the range of experimental interesting temperatures. Experimental values for ξ from inelastic neutron scattering are independent of temperature and have been summarized in Fig. 2 of Ref.²⁰as a function of doping. For optimally doped $YBa_2Cu_3O_{7-x}$ ξ is only little larger than 1 which also agrees with NMR data^{21,22}. This supports the idea that χ_∞ represents a sensible approximation for the spin susceptibility in the optimal and overdoped regime.

IV. PROPERTIES OF Θ_s NEAR THE FERMI SURFACE AND ITS INFLUENCE ON THE TRANSITION TEMPERATURE T_C

A relevant quantitiy for superconductivity is $\Theta(\mathbf{k}, \mathbf{k}', \omega = 0)$ with momenta \mathbf{k} and \mathbf{k}' put to the Fermi surface. Fig. 4 shows this quantitiy for a fixed first momentum at $\mathbf{k} = (2.465, 0.309)$ as a function of the second momentum \mathbf{k}' . \mathbf{k}' moves counterclockwise around the Fermi line passing through the points $X, Y, (\bar{X}, \bar{Y})$ along the positive (negative) x- and y-axis, respectively. The dashed line corresponds to the kernel $g^2\chi_P/8$, using the coupling constant $g = 0.6eV$ from Table II of Ref.⁸. The dot-dashed and solid lines in Fig. 4 describe the kernel Θ_s and the full O(1) kernel Θ calculated in Ref.⁵, respectively. The doping is always $\delta = 0.17$ and J equal to 0.3. The additional factor $1/N$ in Θ_s has been taken into account using the physical value $N = 2$. The curves are not symmetric with respect of X or \bar{X} because the first argument \mathbf{k} has been put to a general point somewhat away from X .

First we note that all three curves have maxima at Y and \bar{Y} , i.e., for momentum transfers of $\mathbf{Q} = (\pi, \pi)$ or of $-\mathbf{Q}$. The dashed and dot-dashed curves correspond to purely repulsive,

the solid one to predominantly repulsive interactions. As a result d-wave pairing is preferred in all three cases. The variation in the solid curve along the Fermi surface, which for d-wave pairing is the relevant quantity, is about two to three times larger than for the dot-dashed curve. This means that the spin-fluctuation mediated interaction is by this factor smaller compared to the sum of all $O(1)$ contributions to the effective interaction. This already indicates that the $1/N$ expansion makes sense insofar that the terms decrease with increasing order in $1/N$. The dot-dashed line in Fig. 4 exhibits some fine structure near the point \bar{Y} which is caused by the splitting of the peak at \mathbf{Q} into incommensurate peaks displaced slightly away from \mathbf{Q} . The appearance of these incommensurate peaks due to the Fermi-surface geometry has been discussed previously in Ref.²³.

The kernel $\Theta(\mathbf{k}, \mathbf{k}', 0)$ represents the effective interaction in the particle-particle channel at zero frequency. The solid line in Fig. 4 thus can be compared with the upper curve in Fig. 8 of Ref.²⁴ which has been obtained from Monte Carlo simulations. Though both kind of curves show minima at the X and maxima at the Y points the energy scale of the curve in Ref.²⁴ is one order of magnitude larger than in our case and also has a large momentum independent part. These differences can roughly be explained by the fact that the energy scale in Ref.²⁴ is set by the Hubbard constant U and in our case by $J(\mathbf{k})$. The parameter values used in Ref.²⁴ thus correspond more to the weak-coupling case whereas we deal with strong-coupling. Fig. 4 also shows that the momentum dependence of the effective interaction is similar to that of the spin susceptibility which determines the momentum dependence of the dashed and dot-dashed curves. However, one cannot conclude from this that the effective interaction is caused by antiferromagnetic spin fluctuations because the solid line does not include them.

The dashed curve in Fig. 4 is at least one order of magnitude larger than the dot-dashed curve, especially, near the point Y . Though both terms describe interactions due to spin fluctuations their strengths differ roughly by one order of magnitude. To understand why these curves are so different in magnitude we characterize the coupling in the large- N expression Eq.(8) by an effective coupling constant \bar{g} . Since both, t and J , depend on the momentum we define \bar{g} by the following average value appropriate for d-wave symmetry

$$\bar{g}^2 = \langle\langle \Theta_s(\mathbf{k}, \mathbf{k}', \omega = 0) \rangle\rangle_3 / \langle\langle \chi^{(0)}(\mathbf{k}, \mathbf{k}', \omega = 0) \rangle\rangle_3. \quad (18)$$

$\langle\langle \dots \rangle\rangle_3$ denotes in the above equation a momentum average over the Fermi line with a weight function with d-wave symmetry. An appropriate weight function is given by the eigenvector associated with the lowest eigenvalue with d-wave symmetry. The explicit form of the corresponding kernel yielding the desired eigenvalues and eigenvectors has been described in Ref.³. This definition can be extended to any momentum-dependent operator. The Fermi surface average is then obtained as the lowest eigenvalue of the associated operator. The dot-dashed and the dotted lines in Fig. 5 show the numerator and the denominator of the right-hand side of Eq.(18) as a function of doping. One concludes from these curves that \bar{g} depends only weakly on the doping and that it is about 0.5 to 1 eV in magnitude. If one puts t to zero in the numerator on the right-hand side of Eq.(18) the ratio is about 0.1 (eV)². This means that \bar{g} is determined essentially by t and given approximately by the full band width. This result is a typical strong-coupling result because the effective coupling constant \bar{g} is determined by the kinetic energy and not by potential interactions. One also concludes from this that the coupling constant $g = 0.6\text{eV}$ used in Ref.⁷ for the coupling between holes

and spin excitations is not too large and thus does not cause the difference in magnitude between the dashed and the dot-dashed curves in Fig. 4. Also shown in Fig. 5 are the lowest eigenvalues of d-wave symmetry for the total kernel of the O(1) theory (solid line), the kernel Θ_s (dot-dashed line, which is identical with the line representing the numerator on the right-hand side of Eq.(18)) and the kernel $g^2\chi_P$ (dashed line). The eigenvalues of the two spin-fluctuation mediated kernels differ by roughly one order of magnitude which reflects the ratio of the corresponding curves in Fig. 4. Using the more realistic value²⁰ $\xi \sim 1$ in χ_P the dashed curve would dramatically move upwards and be near the dotted or dot-dashed curves. Interesting is also that the eigenvalues of the leading order of the large-N theory (solid line) is only about a factor 2 larger than those of Θ_s .

Fig. 6 shows curves for the negative imaginary part of the kernel Θ as a function of frequency. This quantity is the analogue of the familiar function $\alpha^2 F(\omega)$ of Eliashberg theory for conventional superconductivity. The dependences on the momenta \mathbf{k} and \mathbf{k}' have been averaged over the Fermi surface using the lowest eigenvalue of d-wave symmetry of the appropriate operator. The solid line is the result of the large-N theory, omitting the instantaneous, attractive term. The dot-dashed and the dashed lines correspond to the spin-fluctuation mediated interactions described by Θ_s and $g^2\chi_P$, respectively.

The d-wave average $\langle\langle \dots \rangle\rangle_3$ over the Fermi line and the momentum average over the Brillouin zone may yield quite different results as can be seen by comparing the dashed and dot-dashed curves in Fig. 1 with the corresponding curves in Fig. 6. Density of states effect are vital in the average $\langle\langle \dots \rangle\rangle_3$, giving momentum transfer $\mathbf{q} \sim \mathbf{Q}$ a large weight. As a result the dashed and dot-dashed curves in Fig. 6 resemble more the corresponding curves in Fig. 2 than in Fig. 1. The dashed curve in Fig. 6 exhibits a strong maximum around 15 meV and a slow decay towards high energies with a typical decay constant of about 100 meV. Compared to the dashed curve the dot-dashed curve in Fig. 6 assumes everywhere only small values, is rather structureless and has a broad maximum around 0.5 eV. Since the coupling constants \bar{g} and g are of similar magnitude in the two cases the difference between the dashed and dot-dashed curves in Fig. 6 is due to the difference in χ_P and χ_∞ , especially for momenta $\mathbf{q} \sim \mathbf{Q}$. If one restricts oneself to energies between zero and 0.8 eV the integrated spectral weight of the solid curve is much larger than that of the dot-dashed curve. This implies that the next-to-leading contribution in the $1/N$ expansion is substantially smaller than the leading one which gives evidence for the usefulness of the $1/N$ expansion. In the same energy interval the average spectral weight of the solid curve is substantially larger than that of the dashed curve. However, the solid curve becomes strongly negative between 1 and 2 eV. This negative part compensates to a large extent the positive spectral weight between 0 and 0.8 eV if one calculates the real part of the effective interaction. As a result the retarded O(1) contribution to Θ becomes rather small at low frequencies and the attractive instantaneous part causes mainly the superconductivity, as discussed in Ref.⁵. Such a compensation is absent in the two spin fluctuation curves because they are always positive and also very small at high energies.

Using the numerical procedure described in Ref.⁵ to solve the linearized gap equation Eq.(1) we find for T_c the values shown in Fig. 7. The circles describes T_c as a function of δ for the O(1) expression for Θ as discussed in Ref.⁵. If only the new term Θ_s is taken into account the corresponding T_c is given by the crosses. These T_c 's are at least one order of magnitude smaller than the values for T_c using the O(1) expression. In accordance with

that the T_c 's for all terms included in the gap equation (diamonds) are only slightly larger than those calculated solely from the $O(1)$ contribution.

V. IMAGINARY PART OF THE SELF-ENERGY AND RELAXATION RATES

The particle-particle and the particle-hole effective interactions are, except for a possible minus sign in the case of spin fluctuations, identical if the effective interaction is mediated by bosons with energies much smaller than the Fermi energy. T_c , quasi-particle life times and transport relaxation rates are then obtained by taking different Fermi surface averages of the effective interaction. The particle-particle and the particle-hole interactions in $O(1/N)$ of the $t - J$ model are, however, different. Quasi-particle life times and scattering rates are not averages of the function Θ of Eq.(1) but of the corresponding function Θ^{ph} in the particle-hole channel. Following Refs.^{5,12} the $O(1/N)$ contribution to the normal-state self-energy Σ' of the electronic Green's function G , defined in Eq.(10) of Ref.⁵, is given by

$$\Sigma'(k) = \frac{1}{N} \sum_{k'} \Theta^{ph}(k, k') g(k + k'), \quad (19)$$

with

$$\Theta^{ph} = \Theta_1^{ph} + \Theta_2^{ph}, \quad (20)$$

$$\begin{aligned} \Theta_1^{ph}(k, k') = & -\gamma_c(k, k')(t(\mathbf{k} + \mathbf{k}') + J(-\mathbf{k}')) - (t(\mathbf{k} + \mathbf{k}') + J(-\mathbf{k}'))(t(\mathbf{k}) + J(\mathbf{k}'))\chi_{12}(k') \\ & + \gamma_c(k, k') \sum_{r=1}^5 \tilde{E}_r(k) \tilde{\chi}_{2r}(k') - \gamma_c(k, k') \sum_{r=1}^5 \tilde{\chi}_{2r}(k') \sum_{s=1}^5 \tilde{\chi}_{rs}(k') \tilde{E}_s(k) \\ & - \sum_{r,s,t=1}^5 \tilde{S}_r(k'k) \tilde{\chi}_{rs}(k') \tilde{\chi}_{st}(k') \tilde{E}_t(k), \end{aligned} \quad (21)$$

with

$$\tilde{S}_r(k', k) = - \sum_{s=1}^5 (1 + \tilde{\chi}(k'))_{rs}^{-1} \tilde{\chi}_{2s}(k') \gamma_c(k, k'), \quad (22)$$

$$\Theta_2^{ph}(k, k') = g_0^{-1}(k) Q^{-1}(t(\mathbf{k} + \mathbf{k}') + J(-\mathbf{k}')) (L(\begin{smallmatrix} 00 & 00 \\ & k' \end{smallmatrix}) + NL(\begin{smallmatrix} 12 & 21 \\ & k' \end{smallmatrix})). \quad (23)$$

L is the Fourier transform of the equilibrium Green's function of two bosonic operators $X(1)$, $X(2)$, except for a minus sign,

$$L(1, 2) = \langle T(X(1) - \langle X(1) \rangle)(X(2) - \langle X(2) \rangle) \rangle. \quad (24)$$

$g_0(k)$ is the free quasi-particle Green's function $(i\omega_n - \epsilon(\mathbf{k}))^{-1}$ and Q the spectral weight $\langle X^{00}(\bar{1}) \rangle + \langle X^{11}(\bar{1}) \rangle$. At large N the second term in Q could be dropped because it contributes only higher orders in $1/N$ than those considered here. For the transition from large N to the physical value $N = 2$ it is advisable, however, to keep also higher orders in $1/N$ in the inverse spectral weight in order to improve the convergence of the $1/N$ expansion at small

doping. The remaining symbols in Eqs.(21), (22), and (23) have been defined in Eqs.(41-48) of Ref.⁵.

The self-energy Σ' is associated with the physical Green's function G . Taking only Θ_1^{ph} in Eq.(20) into account Eq.(19) defines a different self-energy Σ related to the quasi-particle Green's function g defined in Eq.(15) of Ref.⁵. If k is near the Fermi surface (i.e., $\epsilon(\mathbf{k})$ near the Fermi energy and the frequency $i\omega_n$ small) Θ_2^{ph} of Eq.(23) is small due to the factor $g_0^{-1}(k)$. This means that the two kind of self-energies are essentially equal near the Fermi surface. However they differ considerably far away from the Fermi energy: The imaginary part of Σ' is there always negative definite as it should be in contrast to that of Σ which assumes there in general both signs.

Fig. 8 shows various contributions to the negative imaginary part of Σ' as a function of energy for $t = 0.4eV$, $J/t = 0.3$, $\delta = 0.17$, calculated at very low temperatures. The momentum in the self-energy has always been averaged over the Fermi surface. The dotted line describes the pure spin-flip contribution, i.e., the second term in Eq.(21) and the second L-contribution in Eq.(23). The dot-dashed line in Fig. 8 contains the charge contribution to the self-energy, i.e., the first term in Eq.(21) and the first L-contribution in Eq.(23). The solid line in Fig. 8 contains the contribution of all terms in Θ^{ph} , i.e., the full $O(1)$ contribution of Σ' . First we note that the sum of the dotted and dot-dashed lines in Fig. 8 is not much different from the solid line. This means that the terms 3-5 in Eq.(21) describing mixed charge and spin fluctuations yield only a small contribution to Σ' . The imaginary part of Σ' shows a double peak both for negative and positive frequencies. The peaks at lower frequencies are due to spin, the peaks at higher energies due to collective charge fluctuations. This is in agreement with the properties of the spin and charge excitation spectra of the $t-J$ model²⁵. For relaxation rates and transport only the low-frequency part of the imaginary part of Σ' is relevant. Fig. 8 suggests that this part is mainly determined by spin and only to a lesser degree by charge fluctuations.

Theories for high- T_c superconductors which are based on a retarded, boson-mediated pairing mechanism usually encounter the problem to reconcile the large values for T_c with the rather modest value for the resistivity. Using the leading order of the $1/N$ expansion it was shown⁵ that the obtained values for T_c are comparable with those found in high- T_c superconductors. The question immediately arises whether the same theory (and also theories based on phonon- or spin fluctuation-mediated interactions) are in agreement with the observed low electronic scattering rates in these systems. For this aim we study the quantities $1/\tau$ and $1/\tau_{tr}$ which describe the relaxation of quasi-particles and the momentum relaxation near the Fermi surface, the latter being intimately related to transport. Using our previously defined effective particle-hole interaction Θ^{ph} one obtains²⁶

$$1/\tau = \frac{2}{N} \int_{-\infty}^{\infty} d\epsilon N(\epsilon) \langle\langle \text{Im} \Theta^{ph}(\mathbf{k}, \mathbf{k}' - \mathbf{k}, \epsilon) \rangle\rangle_0 (n_b(\epsilon) + n_F(\epsilon)), \quad (25)$$

$$1/\tau_{tr} = \frac{2}{N} \int_{-\infty}^{\infty} d\epsilon N(\epsilon) \frac{\langle\langle \text{Im} \Theta^{ph}(\mathbf{k}, \mathbf{k}' - \mathbf{k}, \epsilon) (\mathbf{v}(\mathbf{k}) - \mathbf{v}(\mathbf{k}'))^2 \rangle\rangle_0}{\langle\langle (\mathbf{v}(\mathbf{k}) - \mathbf{v}(\mathbf{k}'))^2 \rangle\rangle_0} (n_b(\epsilon) + n_F(\epsilon)), \quad (26)$$

$\langle\langle \dots \rangle\rangle_0$ denotes an average over the Fermi line with a constant eigenvector, i.e., the weight in the line integral around the Fermi line contains only the density of states. Im stands for the imaginary part, $\mathbf{v}(\mathbf{k}) = \partial\epsilon(\mathbf{k})/\partial\mathbf{k}$ is the velocity of the electron at the point

\mathbf{k} . $N(\epsilon)$, $n_B(\epsilon)$ and $n_F(\epsilon)$ denote the density of states, the Bose and the Fermi distribution function, respectively. In the high temperature limit $1/\tau$ and $1/\tau_{tr}$ approach the limits $2\pi T\lambda$ and $2\pi T\lambda_{tr}$, respectively, where λ and λ_{tr} are the corresponding dimensionless coupling strengths. In order to achieve the desired high values for T_c with a spin-fluctuation or phonon mechanism λ has to be roughly between two and three (2.6 in Ref.⁹, 3 in Ref.²⁹, 2.28 using χ_P and the values of Table II, second-last column, of Ref.⁸, 2.9 in Ref.²⁷). On the other hand, infrared and resistivity data in many cuprates near optimal doping lead to a much lower experimental value for λ_{tr} of about 0.3 ± 0.1 , see Table II in Ref.²⁸.

The dashed curves in Figs. 9 and 10 show $1/\tau$ and $1/\tau_{tr}$, respectively, as a function of temperature for the kernel $g^2\chi_P$. The curves are quasilinear above 150 or 200 K corresponding to dimensionless coupling constants λ_P and $\lambda_{tr,P}$ of about 2-3. Such a large value for λ_P is needed in order to reproduce the large value for T_c . The corresponding transport value $\lambda_{tr,P}$, however, is even larger by about 20 per cent. The reason for this is the following: If Θ is momentum independent λ and λ_{tr} are equal. Considering now kernels Θ which depend only on the difference of their momenta, i.e., $\mathbf{k} - \mathbf{k}'$. If Θ shows mainly forward scattering, i.e., if $Im\Theta(\mathbf{k} - \mathbf{k}')$ is large for small momentum and small at large momentum transfers λ_{tr} is smaller than λ . On the other hand if scattering occurs mainly with large momentum transfers λ is smaller than λ_{tr} . Spin-fluctuations are strongest in the region around \mathbf{Q} in momentum space, i.e., at large momentum transfers. As a result $\lambda_{tr,P} > \lambda_P$ in agreement with the slopes in Figs. 9 and 10. We expect that $\lambda_{tr,P} > \lambda_P$ and $\lambda \sim 2 - 3$ are generic values for spin fluctuation models for high- T_c superconductivity. Thus there is a severe discrepancy of about one order of magnitude between theoretical and experimental values for $\lambda_{tr,P}$.

The long-dashed curves in Figs. 9 and 10 describe relaxation rates due to phonons. Following our previous treatment³⁰ we used a Holstein model with a phonon frequency $\omega_0 = 48\text{meV}$ and a dimensionless coupling strength $\lambda_{Ph} = 0.75$ near optimal doping. As discussed in Refs.^{31,30} vertex corrections must be included even in the leading order of the $1/N$ expansion. The resulting vertex, taken at $\omega = 0$, depends strongly on momentum in the region of the considered doping values. This implies that the constant, bare electron-phonon coupling becomes effectively strongly momentum dependent, being large at small and small at large momentum transfers. As a result the phonon contribution to $\lambda_{tr,Ph}$, given essentially by the slope of the long-dashed line in Fig. 10, becomes much smaller³¹ than $\lambda_{Ph} = 0.75$, namely, $\lambda_{tr,Ph} \sim 0.11$. More generally, such a strong reduction in λ_{tr} relative to λ , should occur for all charge but not for spin interactions. This may explain why phonons and impurities play usually no role in transport data though their bare couplings to electrons may not be small³².

The relation between T_c and relaxation rates is quite different in the case of the $1/N$ expansion. The instantaneous part of the kernel is large, for instance, its Fermi surface average in the d-wave channel is -0.48 at $\delta = 0.17$. This term alone would yield a T_c of about the same magnitude as the whole $O(1)$ contribution for Θ . On the other hand, this instantaneous term does not contribute to the momentum relaxation, i.e., it does not enter transport. The solid lines in Figs. 9 and 10 represent the relaxation rates due to Θ^{ph} as given by Eqs.(20-23). The curves are again quasilinear at not too low temperatures. Their absolute values are rather small and correspond to dimensionless coupling constants of $\lambda \sim 0.25$ and $\lambda_{tr} \sim 0.22$. This means that charge and spin fluctuations do not scatter electrons very

efficiently near the Fermi surface. Finally, the long-dashed curves in Figs. 9 and 10 are the relaxation rates due to the spin fluctuation kernel Θ_s of the $1/N$ expansion. Comparing these curves to the dashed curves in Figs. 9 and 10 one recognizes that the leading spin fluctuation contribution, which is of $O(1/N)$ in Θ , yields only small scattering rates, compared to those in spin fluctuation models for high- T_c compounds. The total transport coupling constant is the sum of its electronic and phononic parts and about 0.5 in our model. This value is near the rather universal experimental value of 0.3 ± 0.1^{28} .

VI. CONCLUSIONS

Using a $1/N$ expansion for the $t - J$ model in terms of X operators the $O(1/N)$ contributions to the anomalous self-energy just below T_c and the self-energy in the normal state have been considered and numerically evaluated for typical values of the model parameters. Our treatment is restricted to the optimally doped and the overdoped region defined by the absence of additional instabilities, e.g., towards a flux state. Unlike to the case of phonons or spin fluctuations the resulting effective interactions in the particle-particle and particle-hole channels turn out to be different from each other. We also show how scattering rates relevant to transport can be obtained from the expression for the self-energy. In order to examine the convergence of the $1/N$ expansion and to take into account antiferromagnetic effects we also have included graphs of $O(1/N^2)$ which describe spin-fluctuation mediated contributions to the effective interaction between electrons. Though these terms are only a subset of all $1/N^2$ contributions it seems not unreasonable to assume that they represent the leading corrections to the $O(1/N)$ terms if, as is often believed, spin fluctuations play an important role in the $t - J$ model in the considered doping region.

Our main conclusion is that the leading $O(1/N^2)$ contribution describing spin fluctuations gives only a small correction to the effective interaction and T_c obtained already in the leading order $O(1/N)$. As discussed in Ref.⁵ the effective interaction in $O(1/N)$ contains no RPA-like spin fluctuations. Instead, this effective interaction and thus also d-wave pairing is caused by the instantaneous contribution of the Heisenberg term and by spin flip processes induced by the X operator algebra and thus by the constraint. The reason for the smallness of the $O(1/N^2)$ contribution is that the momentum averaged magnetic susceptibility at large N 's, χ_∞ , is, as a function of frequency, rather structureless and extends over the whole bandwidth. Though the effective coupling constant between electrons and spin excitations is set by t (and not J) the resulting contribution to the imaginary part of the effective interaction (the analogue of $\alpha^2 F$ of the phonon case) is small compared to the spin flip (and charge) contribution obtained in $O(1/N)$. In contrast to that the spin susceptibilities used in spin fluctuations theories such as χ_P of Refs.⁶⁻⁸ is large and strongly peaked at low frequencies. In other words, most of the spectral weight is in this case accumulated at small frequencies of the order of a fraction of J whereas it is rather constant and spread over an energy scale of t in the case of χ_∞ . Available magnetic susceptibility spectra from inelastic neutron scattering in $YBa_2Cu_3O_{7-x}$ refer mostly to the strongly underdoped region and resemble χ_P more than χ_∞ . In optimally doped samples of $YBa_2Cu_3O_{7-x}$ spin scattering is too weak to be detected presently. The obtained experimental upper bound for χ'' , however, suggests in view of the sum rule that χ'' is rather structureless and spreads over an energy scale set by t similar as χ''_∞ does. There is another fundamental difference between calculations based

on $1/N$ expansions and spin fluctuation models: The effective interaction of $O(1/N)$ in the d-wave channel contains strongly pair-breaking charge excitations at high energies of the order t which cancel the contribution of pair-forming low-energy spin flip excitations to a large extent. These pair-breaking terms are entirely neglected in the spin fluctuation models but play an important role for quantitative calculations of T_c in the $1/N$ expansion.

For the same reasons as above we find that the leading spin fluctuation terms of $O(1/N^2)$ modify only little the scattering rates $1/\tau$ and $1/\tau_{tr}$ obtained already in $O(1/N)$. If spin fluctuation terms would dominate and cause the large values of T_c the corresponding scattering rate $1/\tau_{tr}$ would exceed the experimental ones by far. Responsible for this is also the fact that the spin susceptibility is large for large momentum transfers which makes $1/\tau_{tr}$ even larger than $1/\tau$. In the $1/N$ expansion large values for T_c are compatible with small values for $1/\tau_{tr}$: Spin fluctuation terms are small and T_c is to a large extent determined by the instantaneous part of the interaction which does not contribute to relaxation rates. The case of phonons or, more generally, of charge-charge interactions is somewhat different from spin interactions. Here the charge vertex due to correlation effects has to be included already in leading order of the $1/N$ expansion. As a result collective effects dominate and charge interactions are confined to small momenta causing $1/\tau_{tr} \ll 1/\tau$ near optimal doping. This may explain why phonons and impurities play only a minor role in the transport data of optimally doped high- T_c compounds.

Acknowledgement: The authors are grateful to Secyt and the International Bureau of the Federal Ministry for Education, Science, Research and Technology of Germany for financial support (Scientific-technological cooperation between Argentina and Germany, Project No. ARG AD 3P). The first and second author thank the MPI-FKF, Stuttgart, Germany, and the Departamento de Física, Facultad de Ciencias Exactas e Ingeniería, Rosario, Argentina, respectively, for hospitality. The authors also thank P. Horsch for a critical reading of the manuscript.

REFERENCES

- ¹ N.E. Bickers, D.J. Scalapino, and S.R. White, Phys. Rev. Lett. **74**, 961 (1989)
- ² S. Grabowski et al., Europhys. Lett. **34**, 219 (1996)
- ³ A. Greco and R. Zeyher, Europhys. Lett. **35**, 115 (1996)
- ⁴ R. Zeyher and A. Greco, Z. Phys. B **104**, 737 (1997)
- ⁵ R. Zeyher and A. Greco, Eur. Phys. J B **6**, 473 (1998)
- ⁶ P. Monthoux, A. Balatsky, and D. Pines, Phys. Rev. B **46**, 14803 (1992)
- ⁷ P. Monthoux and D. Pines, Phys. Rev. B **47**, 6069 (1993)
- ⁸ P. Monthoux and D. Pines, Phys. Rev. B **49**, 4261 (1994)
- ⁹ J.P. Carbotte, E. Schachinger, and D.N. Basov, Nature **401**, 354 (1999)
- ¹⁰ D.C. Morse and T. Lubensky, Phys. Rev. B **42**, 7794 (1990)
- ¹¹ E. Cappelluti and R. Zeyher, Phys. Rev. B **59**, 6475 (1999)
- ¹² M.L. Kulić and R. Zeyher, Mod. Phys. Lett. B **11**, 333 (1997)
- ¹³ E. Cappelluti and R. Zeyher, Int. J. Mod. Phys. B **13**, 2607 (1999)
- ¹⁴ S.M. Hayden, G. Aeppli, P. Dai, H.A. Mook, T.G. Perring, S.-W. Cheong, Z. Fisk, F. Dogan, and T.E. Mason, Physica B 241-243, 765 (1998)
- ¹⁵ Ph. Bourges, in *The Gap Symmetry and Fluctuations in High Temperature Superconductors*, edited by J. Bok, G. Deutscher, D. Pavuna, and S.A. Wolf, Plenum, New York (1998), p. 349
- ¹⁶ Ph. Bourges, cond-mat/9902067
- ¹⁷ H.F. Fong, P. Bourges, Y. Sidis, L.P. Regnault, J. Bossy, A. Ivanov, D.L. Milius, I.A. Aksay, and B. Keimer, Phys. Rev. B **61**, 14773 (2000)
- ¹⁸ G. Aeppli, S.M. Hayden, P. Dai, H.A. Mook, R.D. Hunt, T.G. Perring, and F. Dogan, phys. stat. sol. (b) **215**, 519 (1999)
- ¹⁹ Y. Sidis et al., Phys. Rev. Lett. **84**, 5900 (2000)
- ²⁰ A.V. Balatsky and P. Bourges, Phys. Rev. Lett. **82**, 5337 (1999)
- ²¹ K.R. Gorny, O.M. Vyaselev, S. Yu, C.H. Pennington, W.L. Hults, and J.L. Smith, Phys. Rev. Lett. **81**, 2340 (1998)
- ²² T. Auler, M. Horvatic, J.A. Gillet, C. Berthier, Y. Berthier, P. Carretta, Y. Kitaoka, P. Ségransan, J.Y. Henry, Physica C 313, 255 (1999)
- ²³ Q. Si, Y. Zha, K. Levin, and J.P. Lu, Phys. Rev. B **47**, 9055 (1993)
- ²⁴ N. Bulut, D.J. Scalapino, and S.R. White, Phys. Rev. B **47**, 2742 (1993)
- ²⁵ L. Gehlhoff and R. Zeyher, Phys. Rev. B **52**, 4635 (1995)
- ²⁶ P.B. Allen and B. Mitrović, Sol. State Physics **37**, 1 (1982)
- ²⁷ R. Zeyher and G. Zwicknagl, Z. Phys. B - Condensed Matter **78**, 175 (1990)
- ²⁸ D.B. Tanner and T. Timusk, in "Physical Properties of High-T_c Temperature Superconductors III", ed. by D.M. Ginsberg, World Scientific Publ. Comp., Singapore, 1992, p. 363
- ²⁹ R.T. Collins et al., Phys. Rev. B **39**, 6571 (1989)
- ³⁰ A. Greco and R. Zeyher, Phys. Rev. B **60**, 1296 (1999)
- ³¹ R. Zeyher and M. Kulić, Phys. Rev. B **53**, 2850 (1996)
- ³² O.K. Andersen, S.Y. Savrasov, O. Jepsen, and A.I. Liechtenstein, J. of Low Temp. Physics **105**, 285 (1996)

FIGURE CAPTIONS

Fig.1: Momentum integrated magnetic susceptibility $\chi''(\omega)$ in units of μ_B^2/eV . Dot-dashed line: $t - J$ model for $N \rightarrow \infty$; dashed line: $\chi''_P(\omega)$ of Ref.⁸; circles: exp. points for $YBa_2Cu_3O_{6.6}$ at $T = 80K$ ¹⁴.

Fig.2: Magnetic susceptibility $\chi''(\mathbf{Q}, \omega)$ for $\mathbf{Q} = (\pi, \pi)$ in units of μ_B^2/eV . Dot-dashed line: $t - J$ model for $N \rightarrow \infty$ multiplied by 10; dashed line: $\chi''_P(\mathbf{Q}, \omega)$ of Ref.⁸; circles: exp. points for $YBa_2Cu_3O_{6.7}$ at $T = 200K$ ¹⁷.

Fig.3: Absolute value of the real part of the susceptibility at $\omega = 0$ versus distance. Circles and diamonds correspond to χ_∞ and χ_P , respectively, at neighboring sites of the square lattice, the dashed and dot-dashed lines to $K_0(x/\xi)$ with $\xi = 2.3$ and $\xi = 1.0$, respectively.

Fig.4: Dependence of the static kernel $\Theta(\mathbf{k}, \mathbf{k}', 0)$ on the second momentum \mathbf{k}' along the Fermi line for a fixed first momentum $\mathbf{k} = (2.465, 0.309)$; solid line: $O(1)$ contrib.; dot-dashed line: $O(1/N)$ contrib.; dashed line: $g^2\chi_P$ divided by 8.

Fig.5: Lowest eigenvalue of static kernels in Γ_3 (d-wave) symmetry; solid, dashed, dot-dashed, and dotted lines correspond to $O(1)$ of Θ , $g^2\chi_P$, the numerator, and denominator of Eq.(18), respectively. The dot-dashed curve corresponds at the same time to Θ_s .

Fig.6: Negative imaginary part of the d-wave projected kernel $\Theta_3(\omega + i\eta)$ as a function of the frequency; solid, dot-dashed, and dashed lines correspond to the contributions of $O(1)$, $O(1/N)$, and $g^2\chi_P$ to Θ_3 , respectively.

Fig.7: Transition temperature T_c in Kelvin as a function of doping; circles, crosses, and diamonds correspond to the contributions of $O(1)$, $O(1/N)$, and $O(1) + O(1/N)$, respectively.

Fig.8: Negative imaginary part of the $O(1/N)$ electronic self-energy as a function of energy with the momentum averaged over the Fermi surface. Dot-dashed, dashed, and solid lines describe the charge, spin and total contributions, respectively.

Fig.9: Quasi-particle relaxation rate $1/\tau$ as a function of temperature. Dashed, long-dashed, solid, and dot-dashed lines correspond to χ_P , an electron-phonon model, and the $O(1/N)$ and $O(1/N^2)$ contributions to the self-energy of the $t - J$ model, respectively.

Fig.10: Transport relaxation rate $1/\tau_{tr}$ as a function of temperature. Dashed, long-dashed, solid, and dot-dashed lines have been calculated from χ_P , an electron-phonon model, and the $O(1/N)$ and $O(1/N^2)$ contributions to the self-energy of the $t - J$ model, respectively.

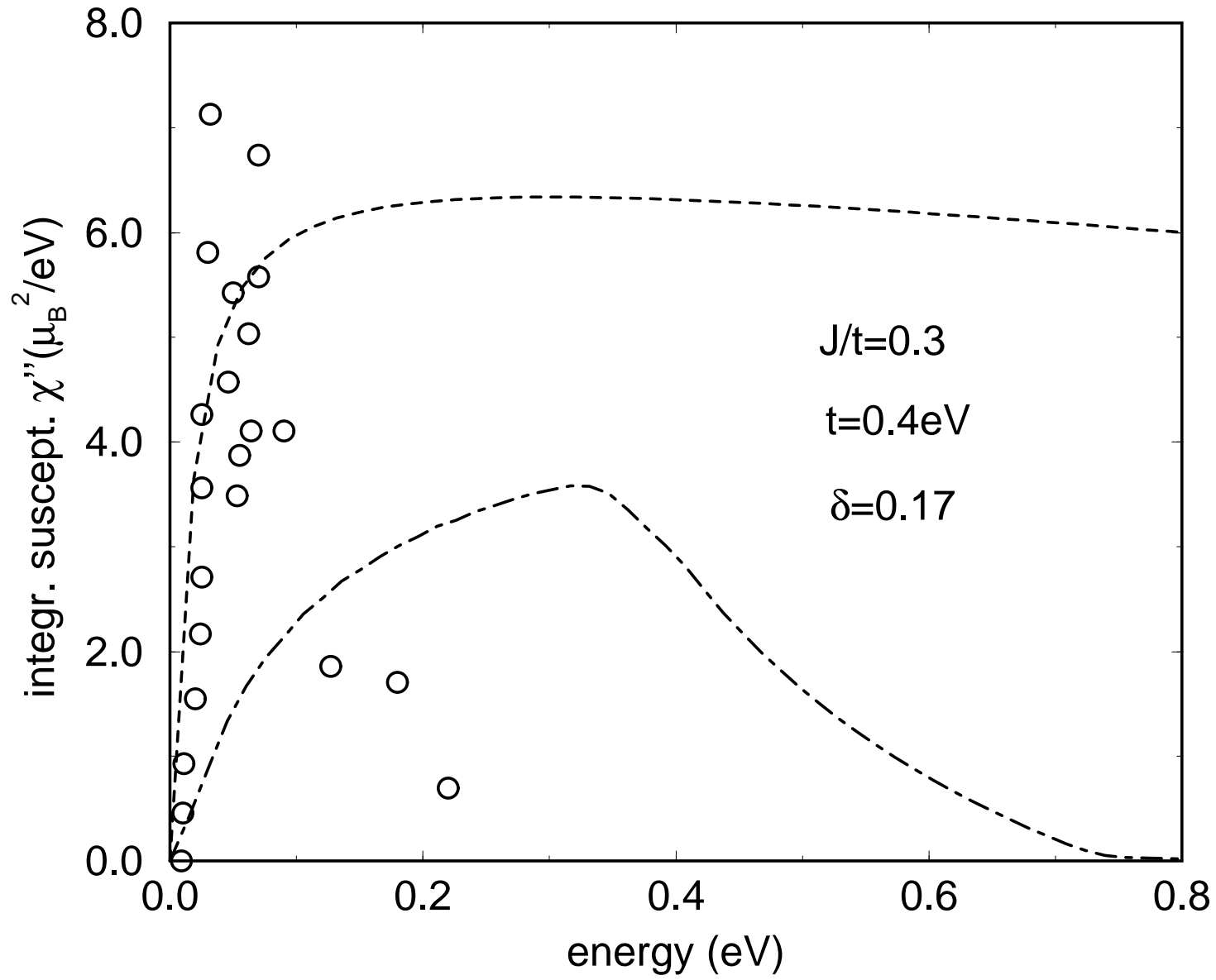


FIG. 2.

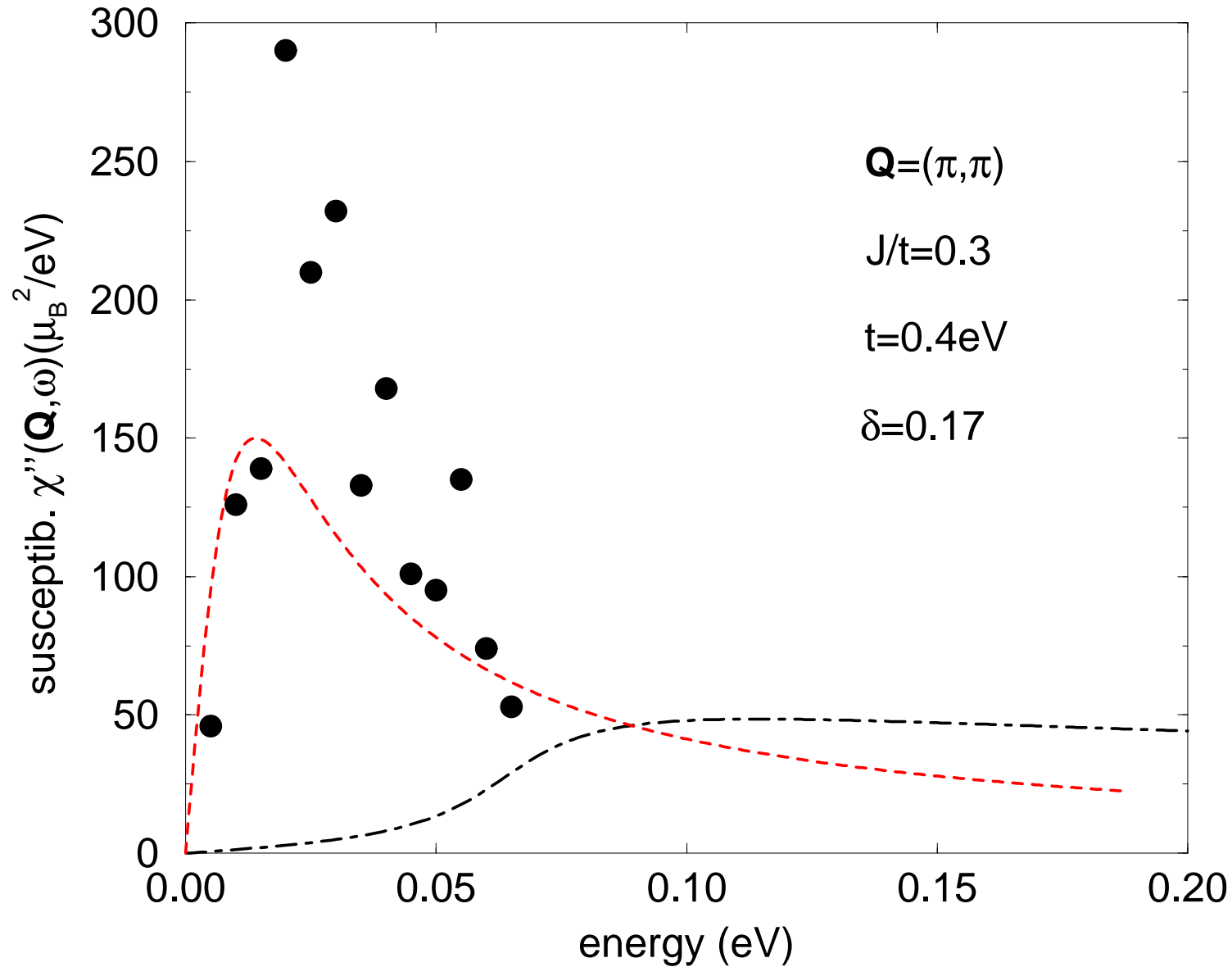


FIG. 3.

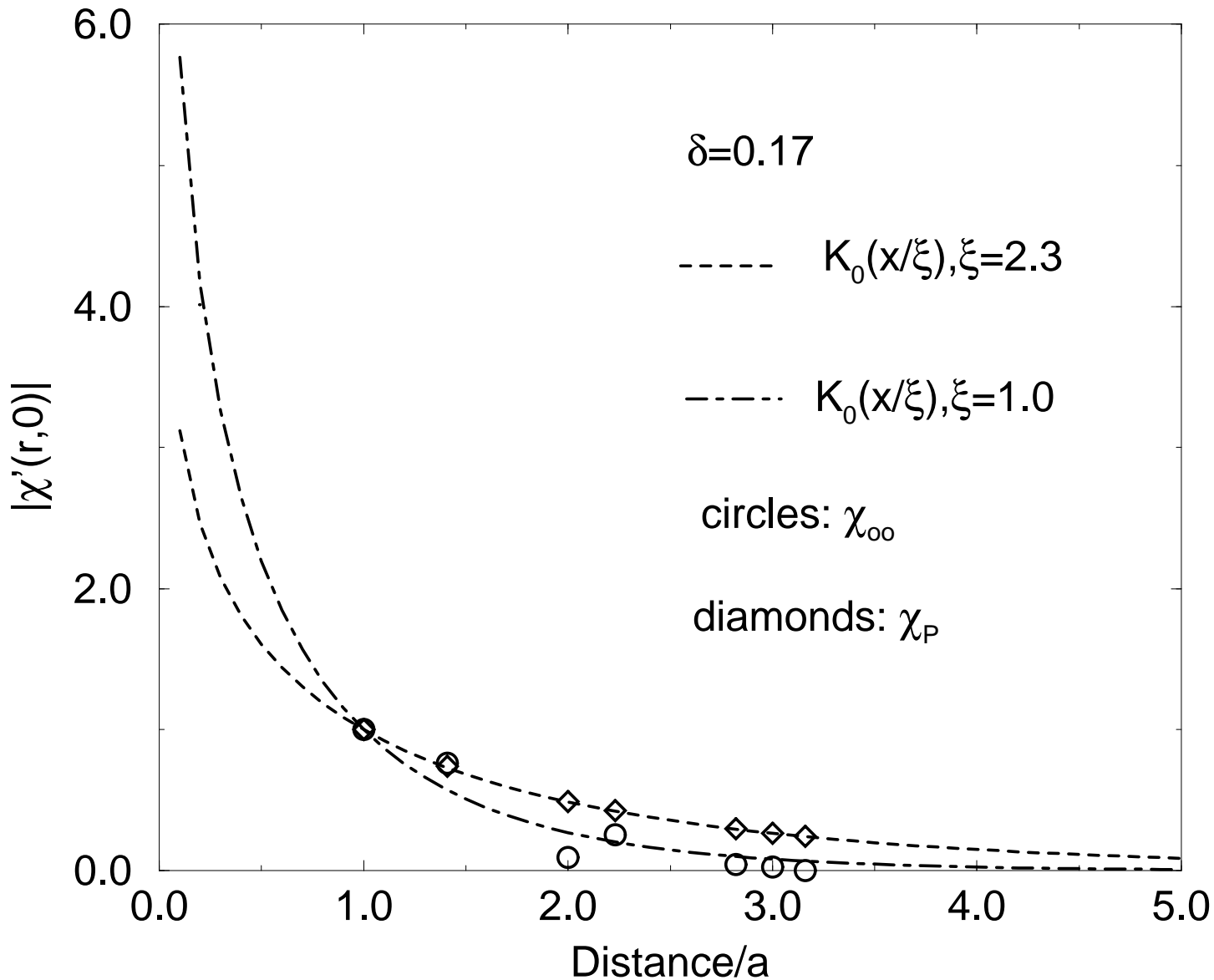


FIG. 4.

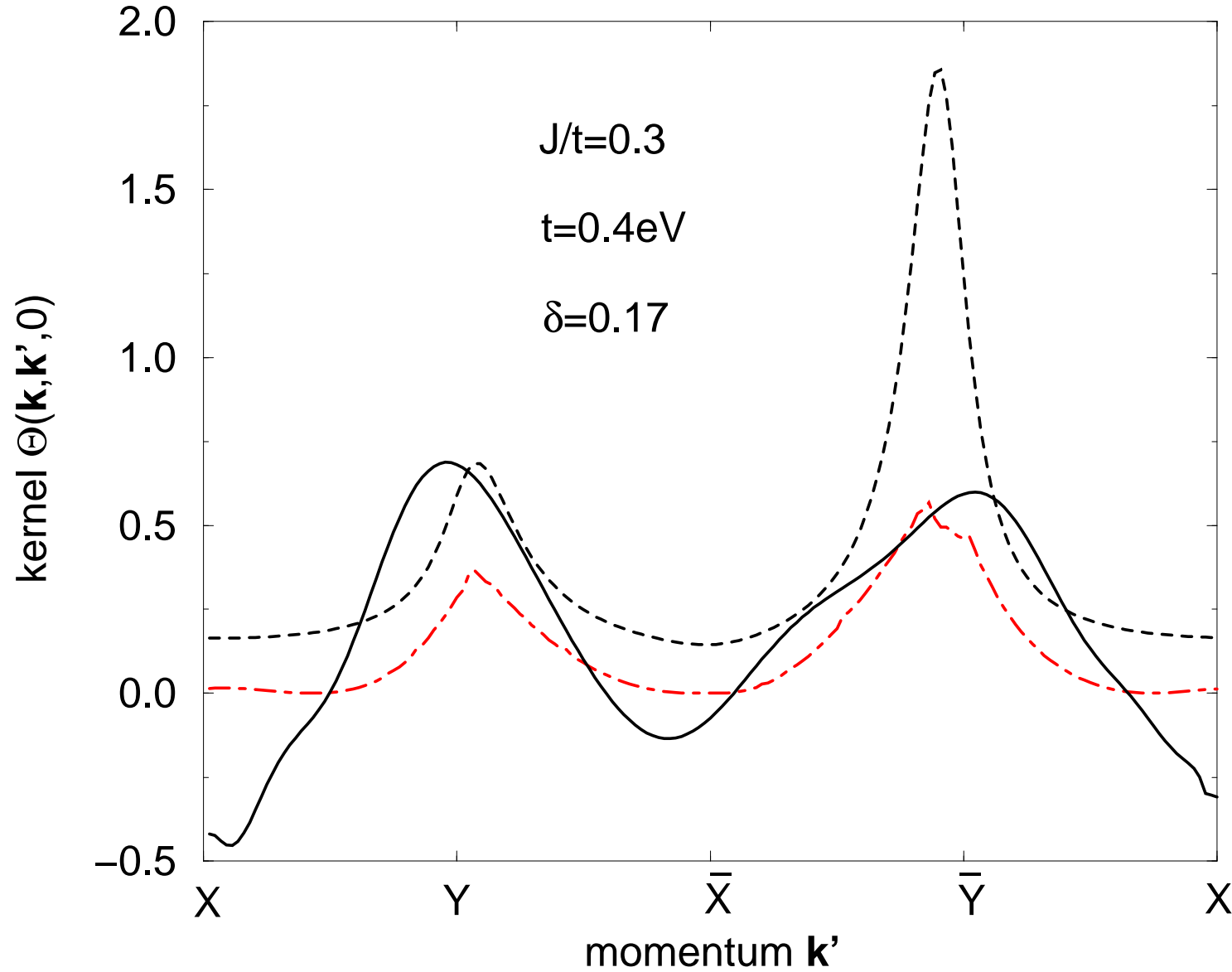
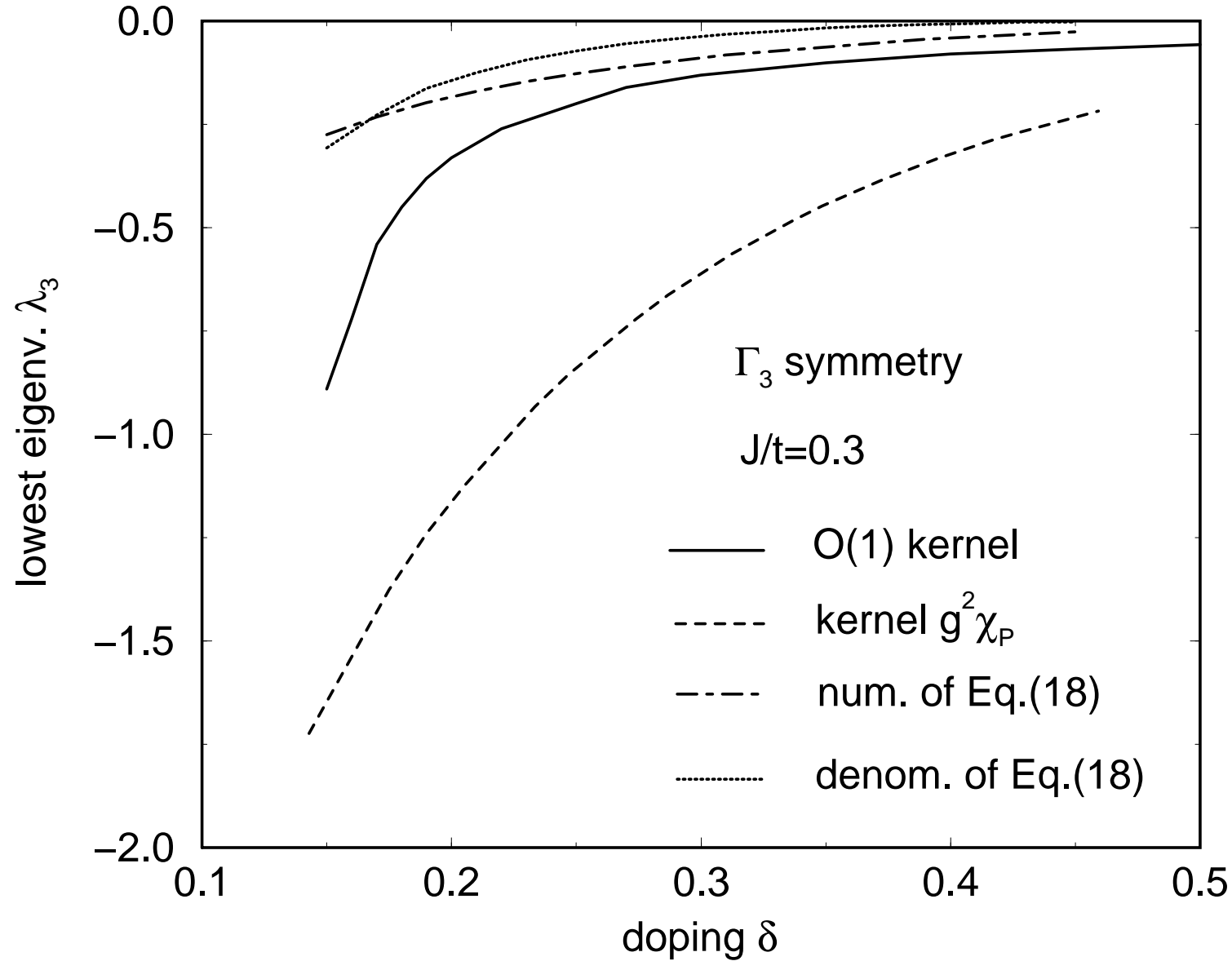


FIG. 5.



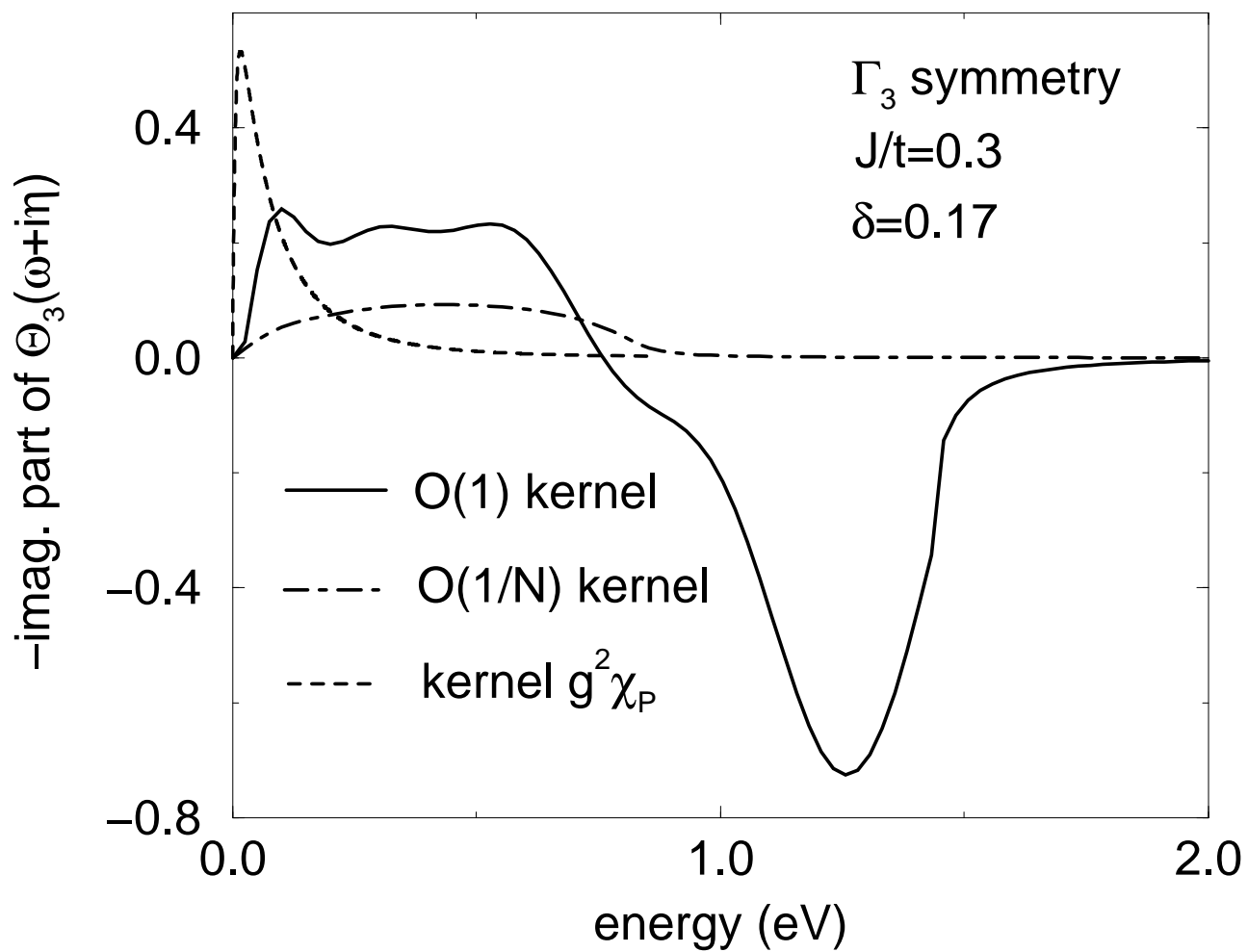


FIG. 6.

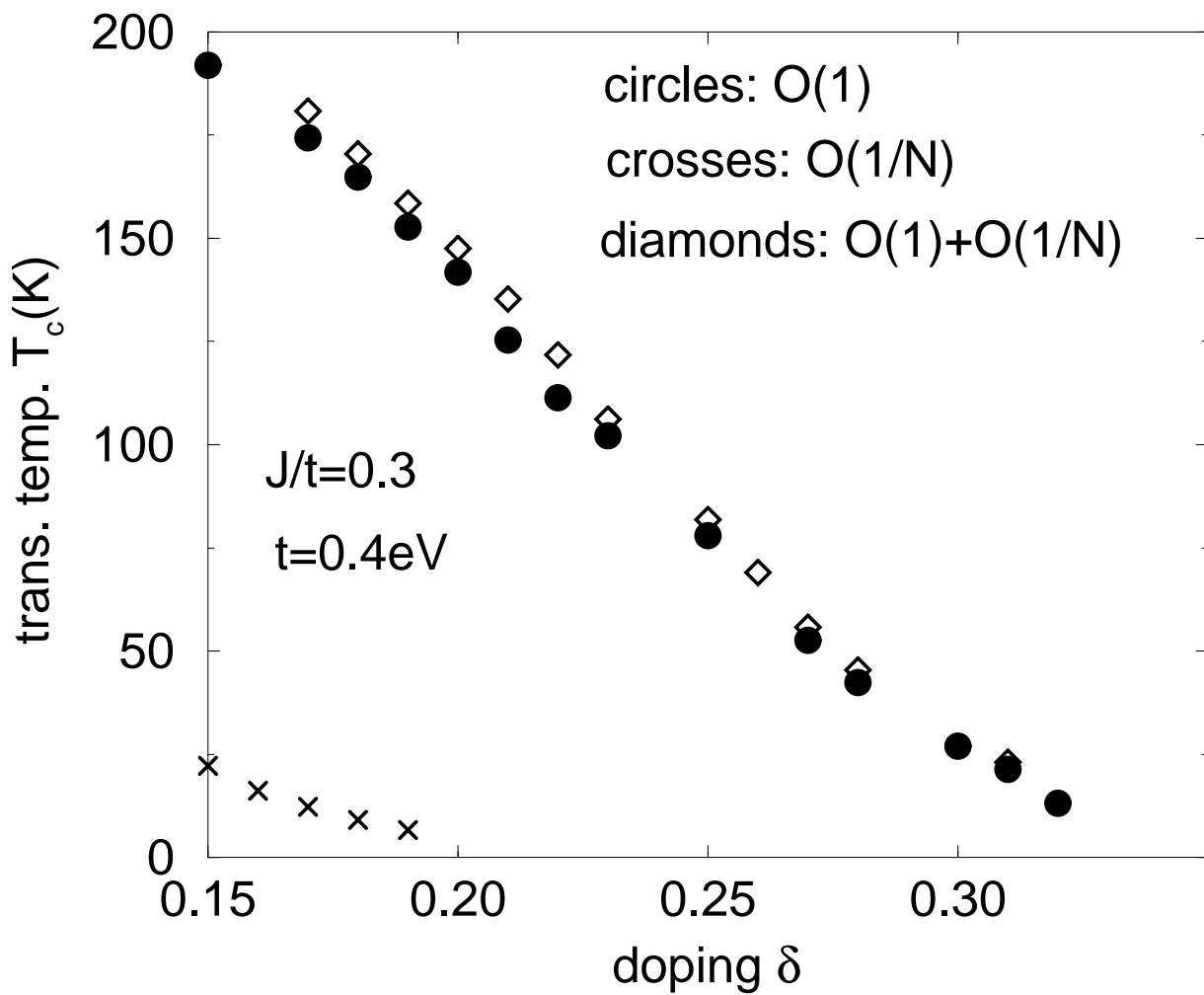


FIG. 7.

FIG. 8.

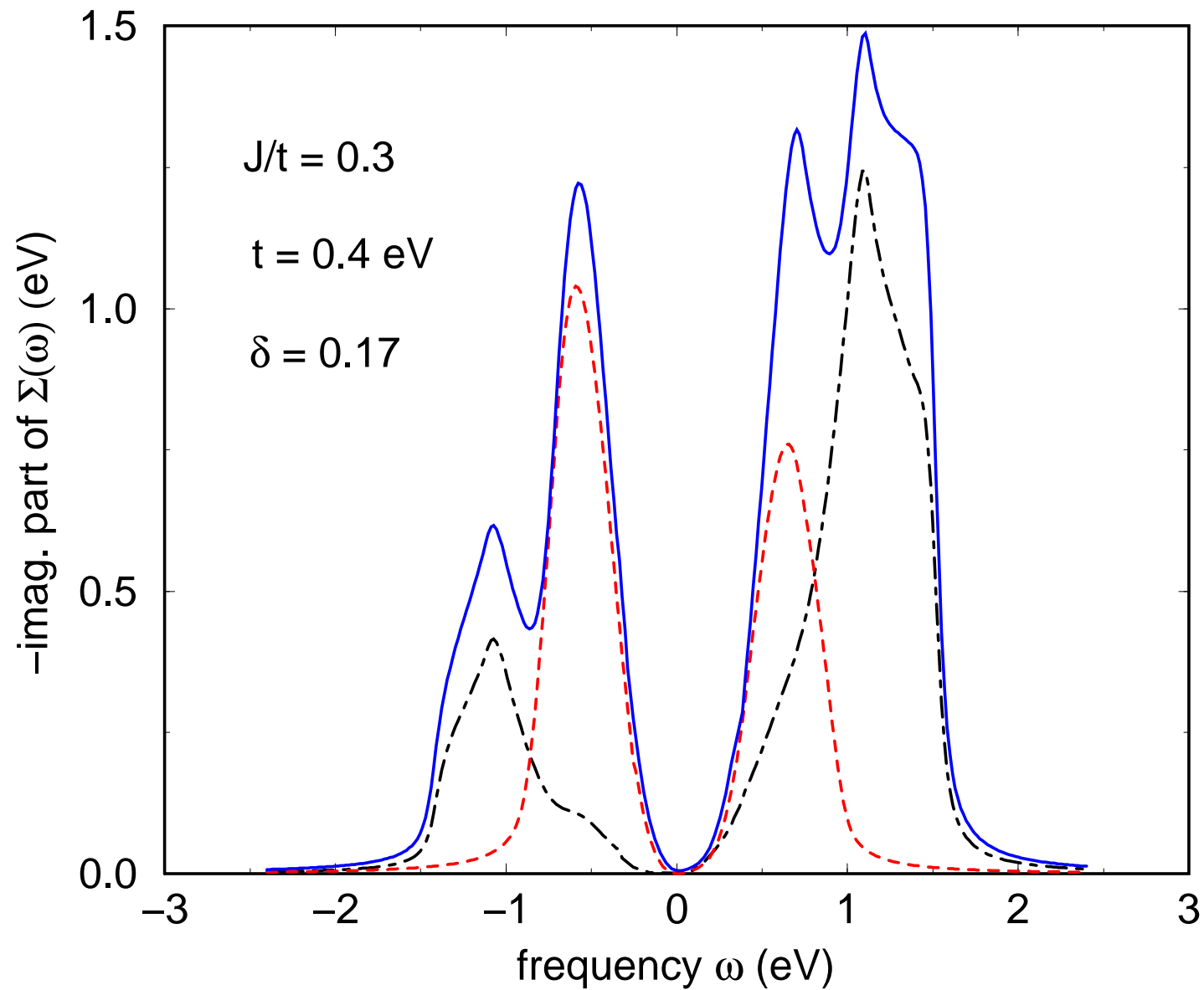


FIG. 9.

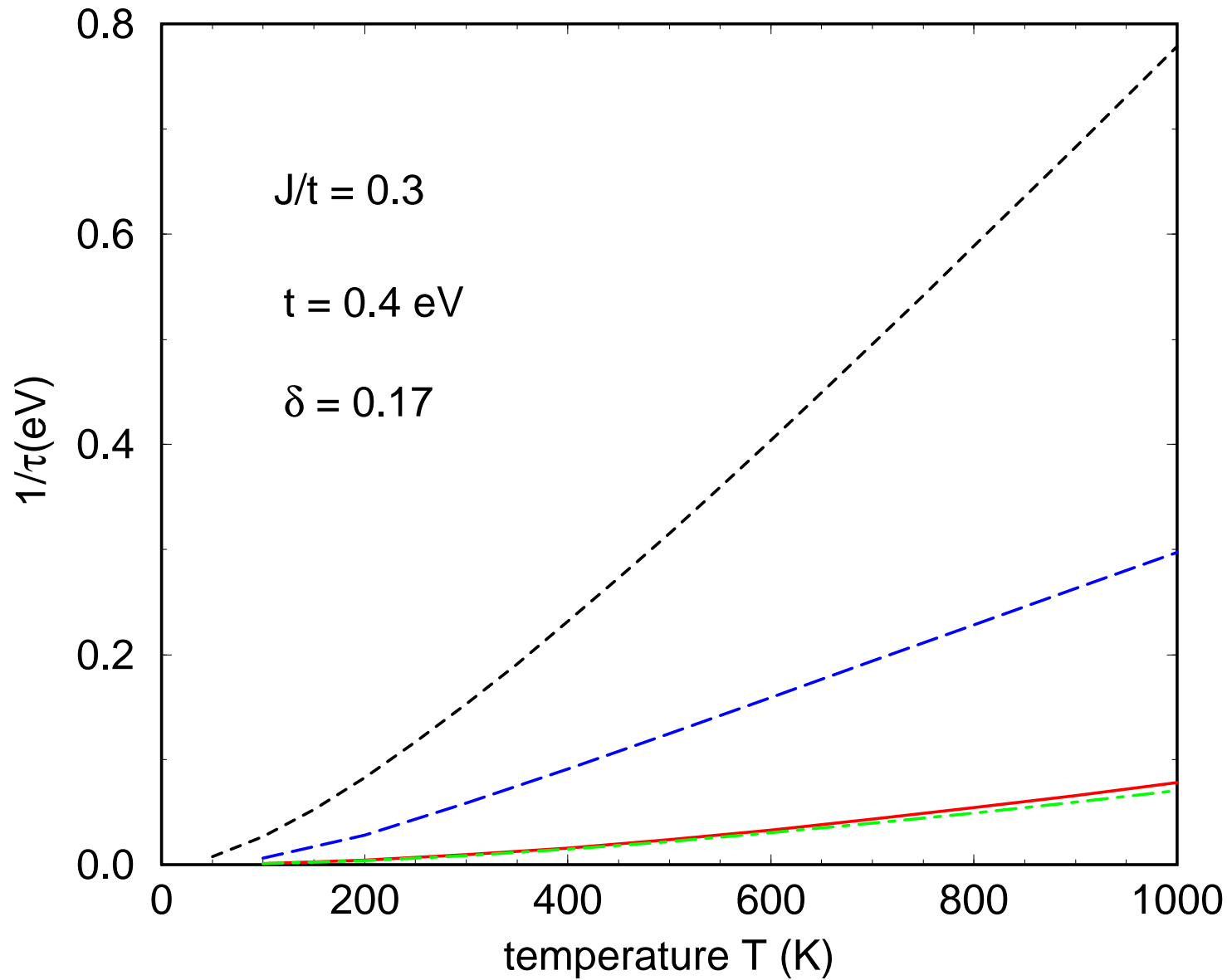


FIG. 10.

